JOURNAL OF GUIDANCE, CONTROL, AND DYNAMICS
Vol. 30, No. 5, September–October 2007

Near-Optimal Missile Avoidance Trajectories via Receding Horizon Control

Janne Karelahti,* Kai Virtanen,† and Tuomas Raivio‡
Helsinki University of Technology, 02015 HUT, Espoo, Finland

DOI: 10.2514/1.26024

This paper introduces a receding horizon control scheme for obtaining near-optimal controls in a feedback form for an aircraft trying to avoid a closing air-to-air missile. The vehicles are modeled as point masses. Rotation kinematics of the aircraft are taken into account by limiting the pitch and roll rates as well as the angular accelerations of the angle of attack and the bank angle. The missile uses proportional navigation and it has a boost-sustain propulsion system. In the proposed scheme, the optimal controls of the aircraft over a short planning horizon are solved online by the direct shooting method at each decision instant. Thereafter, the state of the system is updated by using only the first controls in the sequence, and the process is repeated. The performance measure defining the objective of the aircraft can be chosen freely. In this paper, six performance measures consisting of the capture time, closing velocity, miss distance, gimbal angle, tracking rate, and control effort of the missile are considered. The quality of the receding horizon solutions computed by the scheme is validated by comparing them to the off-line computed optimal open-loop solutions.

I. Introduction

IN AIR combat, the avoidance of guided missiles is extremely important for the survival. Obviously, the best way to avoid a missile is to prevent suitable launch conditions by staying out of the kinematic range or the firing envelope [1] of the missile. If this is not possible, the missile may still be avoided under some conditions by proper exploitation of the missile system weaknesses. Such weaknesses include limited propulsion phase, aerodynamic and structural performance limits, delay in the missile guidance system, and limits of the missile seeker head.

Concerning the design of a guidance scheme for the missile avoidance, it is important to acknowledge that due to many uncertainties related to the pursuit–evasion setting, the controls of the aircraft should be obtained in a feedback form. Near-optimal feedback solutions can be obtained, for example, by neural networks [2] or receding horizon control [3]. A downside of neural networks is that for high-dimensional systems, a plethora of open-loop optimal trajectories must be solved off-line and stored for the adjustment of the neural network parameters. For the problem at hand, this would be practically impossible due to the abundance of possible initial states. In receding horizon control, the controls related to the current state are computed online that effectively eliminates the above disadvantage. Although applied traditionally in the process industry [4], receding horizon control has been recently used also in the numerical solution of various air combat related problems [5,6].

This paper introduces a new receding horizon control scheme for solving a three-dimensional pursuit–evasion problem between a medium range air-to-air missile and a fighter aircraft. Although the vehicles are modeled as point masses, rotational kinematics of the aircraft are taken into account by limiting the pitch and roll rates as well as the angular accelerations of the angle of attack and bank angle. Rotational dynamics of the missile are considered negligible because they are faster than that of the aircraft. The missile is guided by a feedback control law, proportional navigation [7], and it has a boost–sustain propulsion system. The scheme can be applied with various performance measures that exploit different aspects of the missile system, enabling the selection of the most suitable evasion strategy for a given combat state.

Probably the most common performance measure in pursuit–evasion problems is the capture time. In a game setting [8], the pursuer tries to minimize the time of capture whereas the evader tries to maximize it. If the pursuer uses a feedback guidance law, the problem reduces to a one-sided optimal control problem [9] in which the evader maximizes the final time. Another widely studied, undeniably the most relevant performance measure considering the missile avoidance is the miss distance. Because of the more complex nature of the latter problem, usually only planar [10] or otherwise simplified dynamics [11] have been studied. Optimal open-loop solutions for more realistic three-dimensional settings have been solved by direct methods [12]. Efficiency of some well-known evasion maneuvers and suboptimal feedback control laws have been studied by simulation with three-dimensional dynamics [13].

In addition to the capture time and the miss distance, a number of suitable performance measures are available that have received less attention in the open literature, such as closing velocity [14], gimbal angle [15], angular tracking rate [16], and control effort [17] of the missile. The utilization of the first mentioned criterion is justified by the studies of endgame analysis (see, e.g., [18]) which show that the ability of the target to avoid the missile depends strongly on the closing velocity of the missile. Secondly, although modern missile seekers have relatively high gimbal angle and angular tracking rate limits, they may be exceeded under some conditions resulting in a missile lock-off. Finally, the missile can be driven uncontrollable by exhausting the power supply available to the missile control system.

In receding horizon control, the controls are optimized over a short planning horizon at each decision instant. The state of the system is then updated by applying the optimal controls at the current state. By repeating the computations at each decision instant, a suboptimal state dependent feedback solution is obtained. In this paper, the controls of the aircraft over the planning horizon are optimized by using the direct shooting method where the control variables are parameterized and the state equations are integrated explicitly [19]. The time domain over the planning horizon is discretized so that the time interval is increased toward the end of the planning horizon. This enables application of longer planning horizons with less number of time disretization points which reduces solution times. An

Presented as Paper 6312 at the AIAA Guidance, Navigation, and Control Conference and Exhibit, Keystone, Colorado, 21–24 August 2006; received 20 June 2006; accepted for publication 16 February 2007.

*Researcher, Systems Analysis Laboratory, P.O. Box 1100; janne.karelahti@hut.fi. Member AIAA.

†Teaching Research Scientist, Systems Analysis Laboratory, P.O. Box 1100; kai.virtanen@hut.fi.

‡Adjunct Professor, Systems Analysis Laboratory, P.O. Box 1100; tuomas.raivio@hut.fi.

important aspect in receding horizon control is the selection of a suitable approximation for the optimal cost to go over the remaining flight time. The selection can be carried out by using, for example, the problem approximation, the heuristic cost-to-go approximation, or the rollout approach, see, for example, [20]. In this paper, the problem approximation and the heuristic approach are applied, for example, due to their superiority with respect to the computation time.

The scheme is demonstrated with the six criteria discussed above. The performance of the introduced scheme is validated by comparing the receding horizon solutions to the optimal open-loop solution over the entire flight time for each performance measure. The optimal open-loop solutions are computed off-line by the direct multiple shooting method [21]. The comparison is carried out for a large set of initial states and planning horizons.

The paper is structured as follows. In the following section, the aircraft and the missile models are presented. The pursuit–evasion problem along with the performance measures are formulated in Sec. III. The receding horizon control scheme is introduced in Sec. IV, followed by numerical examples in Sec. V. The aspects and the usability of the scheme are discussed in Sec. VI. Finally, concluding remarks appear in Sec. VII.

II. Vehicle Models

The optimal control problem formulation of the pursuit–evasion problem used in this paper is based on the following assumptions:

1) The aircraft and the missile receive accurate state information. Moreover, the aircraft has complete knowledge of the missile model.

2) The vehicles are modeled as point masses. The aircraft maneuverability is limited by the maximum pitch and roll rates as well as the maximum angular accelerations of the angle of attack and the bank angle.

3) The aircraft responds instantaneously to control commands.

4) The missile is guided by proportional navigation.

5) The missile has two independent guidance channels perpendicular to each other in a plane normal to the velocity vector of the missile.

6) The missile has a single-lag guidance system.

7) The missile has a boost–sustain propulsion system.

A. Aircraft Model

The motion of the aircraft is described by the following system of differential equations [22]:

$$\dot{x}_a = v_a \cos\gamma_a \cos\chi_a \tag{1}$$

$$\dot{y}_a = v_a \cos\gamma_a \sin\chi_a \tag{2}$$

$$\dot{h}_a = v_a \sin\gamma_a \tag{3}$$

$$\dot{\gamma}_a = \frac{1}{m_a v_a}\{[L_a(\alpha, h_a, v_a, M(h_a, v_a)) + \eta T_{\max}(h_a, M(h_a, v_a))\sin\alpha]\cos\mu - m_a g\cos\gamma_a\} \tag{4}$$

$$\dot{\chi}_a = \frac{1}{m_a v_a \cos\gamma_a}[L_a(\alpha, h_a, v_a, M(h_a, v_a)) + \eta T_{\max}(h_a, M(h_a, v_a))\sin\alpha]\sin\mu \tag{5}$$

$$\dot{v}_a = \frac{1}{m_a}[\eta T_{\max}(h_a, M(h_a, v_a))\cos\alpha - D_a(\alpha, h_a, v_a, M(h_a, v_a))] - g\sin\gamma_a \tag{6}$$

where x_a and y_a refer to the horizontal coordinates and h_a to the altitude of the aircraft. The remaining three state variables are the flight path angle γ_a, the heading angle χ_a, and the velocity v_a. The aircraft is guided with the angle of attack α, the bank angle μ, and the throttle setting η.

The acceleration due to the gravity g and the mass of the aircraft m_a are assumed constant. $T_{\max}(\cdot)$ denotes the maximum available thrust force directed along to the centerline axis of the aircraft, $L_a(\cdot)$ the lift force, $D_a(\cdot)$ the drag force, and $M(\cdot)$ the Mach number. The lift force is given by

$$L_a(\alpha, h_a, v_a, M(h_a, v_a)) = C_{L_a}(\alpha, M(h_a, v_a))S_a q(h_a, v_a) \tag{7}$$

where $C_{L_a}(\cdot)$ is the lift coefficient and S_a the reference wing area of the aircraft. The dynamic pressure is

$$q(h_a, v_a) = \tfrac{1}{2}\varrho(h_a)v_a^2 \tag{8}$$

where the air density $\varrho(h_a)$ is taken from the International Standard Atmosphere. The drag force is of the form

$$D_a(\alpha, h_a, v_a, M(h_a, v_a)) = C_{D_a}(\alpha, M(h_a, v_a))S_a q(h_a, v_a) \tag{9}$$

where $C_{D_a}(\cdot)$ denotes the total drag coefficient of the aircraft. This as well as the lift coefficient and the maximum thrust of the aircraft is given as tabular data and approximated with suitable continuously differentiable functions.

The control variables are constrained as

$$0 \le \alpha \le \alpha_{\max}, \qquad 0 \le \eta \le 1, \qquad -\infty \le \mu \le \infty \tag{10}$$

In addition, the pitch and the roll rates are constrained by

$$|\dot{\alpha} + \dot{\gamma}_a \cos\mu + \dot{\chi}_a \cos\gamma_a \sin\mu| - Q_{\max} \le 0 \tag{11}$$

and

$$|\dot{\mu}| - P_{\max}(\alpha, h_a, M(h_a, v_a)) \le 0 \tag{12}$$

respectively, where the maximum pitch rate $Q_{\max}$ and the maximum roll rate $P_{\max}(\cdot)$ are aircraft specific values. For the derivation of Eq. (11), see [18]. Moreover, the angular accelerations of the angle of attack and the bank angle are constrained by

$$|\ddot{\alpha}| - \ddot{\alpha}_{\max} \le 0 \tag{13}$$

and

$$|\ddot{\mu}| - \dot{P}_{\max} \le 0 \tag{14}$$

where the maximum angular accelerations of the angle of attack $\ddot{\alpha}_{\max}$ and the bank angle $\dot{P}_{\max}$ are assumed constant.

To avoid stall, the angle of attack must be chosen so that the lift coefficient does not exceed an aircraft specific value $C_{L_a,\max}(\cdot)$ at a given altitude and velocity, that is,

$$C_{L_a}(\alpha, M(h_a, v_a)) - C_{L_a,\max}(M(h_a, v_a)) \le 0 \tag{15}$$

The load factor defined in the wind coordinate system as

$$n_a(\alpha, h_a, v_a) = \frac{L_a(\alpha, h_a, v_a, M(h_a, v_a))}{m_a g} \tag{16}$$

is limited by the structure of the aircraft. This imposes another constraint related to the angle of attack, altitude, and velocity:

$$n_a(\alpha, h_a, v_a) - n_{a,\max} \le 0 \tag{17}$$

In addition, the altitude and the dynamic pressure are constrained by

$$h_{a,\min} - h_a \le 0 \tag{18}$$

and

$$q(h_a, v_a) - q_{\max} \le 0 \tag{19}$$

where $h_{a,\min}$ and $q_{\max}$ refer to the minimum altitude and the maximum dynamic pressure of the aircraft, respectively.

B. Missile Model

The motion of the missile is described by

$$\dot{x}_m = v_m \cos\gamma_m \cos\chi_m \tag{20}$$

$$\dot{y}_m = v_m \cos\gamma_m \sin\chi_m \tag{21}$$

$$\dot{h}_m = v_m \sin\gamma_m \tag{22}$$

$$\dot{\gamma}_m = \frac{1}{v_m}[a_p - g\cos\gamma_m] \tag{23}$$

$$\dot{\chi}_m = \frac{a_y}{v_m \cos\gamma_m} \tag{24}$$

$$\dot{v}_m = \frac{1}{m_m(t)}[T_m(t) - D_m(a, h_m, v_m, M(h_m, v_m))] - g\sin\gamma_m \tag{25}$$

$$\dot{a}_p = \frac{1}{\tau(h_m, M(h_m, v_m))}(a_{pc} - a_p) \tag{26}$$

$$\dot{a}_y = \frac{1}{\tau(h_m, M(h_m, v_m))}(a_{yc} - a_y) \tag{27}$$

The interpretation of the first six state variables is similar to those of the aircraft model. The remaining two state variables a_p and a_y denote the pitch and yaw acceleration components of the missile which are orthogonal to the velocity vector of the missile, whereas $\tau(\cdot)$ is the time constant of the guidance system. The commanded accelerations a_{pc} and a_{yc} depend on the guidance law. The mass of the missile $m_m(t)$ and the thrust force $T_m(t)$ are given as tabular data. The drag force of the missile is given by

$$D_m(a, h_m, v_m, M(h_m, v_m)) = C_{D_m}(a, M(h_m, v_m))S_m q(h_m, v_m) \tag{28}$$

where the drag coefficient $C_{D_m}(\cdot)$ is given as a function of the total lateral acceleration instead of the total angle of attack.

The commanded accelerations are given by

$$a_{ic} = \begin{cases} a_{i\mathrm{PN}} \min\{a_{n,\max}, a_{C_{L,\max}}\}/a_{\mathrm{PN}}, & \text{if } a_{\mathrm{PN}} > \min\{a_{n,\max}, a_{C_{L,\max}}\} \\ a_{i\mathrm{PN}}, & \text{otherwise} \end{cases} \tag{29}$$

where

$$a_{\mathrm{PN}} = \sqrt{a_{p\mathrm{PN}}^2 + a_{y\mathrm{PN}}^2} \tag{30}$$

and the acceleration components $a_{i\mathrm{PN}}$, $i = p, y$ are given by proportional navigation that tries to steer the missile so that the angular rate of the line-of-sight vector from the missile to the target is driven toward zero. Especially in ideal proportional navigation [23] applied in this paper, the commanded acceleration vector is given by

$$\mathbf{a}_c = N'\boldsymbol{\omega} \times \mathbf{v}_c \tag{31}$$

where N' is the navigation constant and

$$\boldsymbol{\omega} = \frac{\mathbf{r} \times (-\mathbf{v}_c)}{\mathbf{r} \cdot \mathbf{r}} \tag{32}$$

is the rotation of the line-of-sight vector due to the closing velocity

$$\mathbf{v}_c = -\dot{\mathbf{r}} = [\dot{x}_m - \dot{x}_a \quad \dot{y}_m - \dot{y}_a \quad \dot{h}_m - \dot{h}_a]^T \tag{33}$$

The pitch and yaw acceleration components are obtained by projecting the commanded acceleration vector on the respective axes as

$$a_{p\mathrm{PN}} = \mathbf{a}_c \cdot \mathbf{e}_{a_p} + g\cos\gamma_m \tag{34}$$

$$a_{y\mathrm{PN}} = \mathbf{a}_c \cdot \mathbf{e}_{a_y} \tag{35}$$

where the normalized pitch and yaw components of the acceleration vector are given by

$$\mathbf{e}_{a_p} = \begin{bmatrix} -\sin\gamma_m \cos\chi_m & \sin\gamma_m \sin\chi_m & \cos\gamma_m \end{bmatrix}^T \tag{36}$$

and

$$\mathbf{e}_{a_y} = \begin{bmatrix} -\sin\gamma_m & \cos\gamma_m & 0 \end{bmatrix}^T \tag{37}$$

respectively. The last term of Eq. (34) compensates the gravity. The commanded accelerations are limited to values not imposing structural damage or stall, that is, the total commanded acceleration is not allowed to exceed either of the following limits:

$$a_{n,\max} = g n_{m,\max} \tag{38}$$

where $n_{\max}$ is the maximal load factor permitted by the structure of the missile and

$$a_{C_{L_m},\max} = C_{L_m,\max}(h_m, M(h_m, v_m))S_m q(h_m, v_m)/m_m(t) \tag{39}$$

The stall limit $C_{L_m,\max}(\cdot)$, the drag coefficient $C_{D_m}(\cdot)$, and the time constant of the guidance system $\tau(\cdot)$ are given as tabular data and approximated by suitable smooth functions.

III. Pursuit–Evasion Problem

The pursuit–evasion problem between the missile and the aircraft is next formulated as an optimal control problem. The aircraft minimizes/maximizes the performance measure

$$J(\mathbf{u}) = \int_{t_0}^{t_f} L(\mathbf{x}, \mathbf{u}, t)\,\mathrm{d}t + \varphi(\mathbf{x}_f, t_f) \tag{40}$$

subject to

$$\dot{\mathbf{x}} = \mathbf{f}(\mathbf{x}, \mathbf{u}, t), \qquad \mathbf{x}(t_0) = \mathbf{x}_0 \tag{41}$$

$$\mathbf{g}(\mathbf{x}, \mathbf{u}, \dot{\mathbf{u}}, \ddot{\mathbf{u}}) \le \mathbf{0} \tag{42}$$

$$h(\mathbf{x}_f) = 0 \tag{43}$$

The state vector $\mathbf{x}$ contains the states of the aircraft and the missile, $\mathbf{u}$ is the control vector of the aircraft, and $\mathbf{x}_0$ denotes the initial states of the aircraft and the missile. The differential equations (41) describing the dynamics of the vehicles refer to Eqs. (1–6) and (20–27). Constraints (42) limiting the controls and preventing, for example, stalling and exposure to excessive accelerations refer to Eqs. (10–19). Terminal constraint (43) defines the free final time t_f.

It should be noted that the above optimal control problem does not necessarily have a solution for an arbitrary initial state. For example, if the missile is launched outside its firing envelope, the missile cannot reach an optimally outrunning aircraft. On the other hand, if the aircraft prefers to exploit a particular aspect of the missile's overall system design instead of outrunning, the missile may reach the aircraft with the same initial state. Hence, the set of feasible initial states depend on the utilized performance measure as well as the missile's target set defined by Eq. (43).

In the following, the first two performance measures result in outrun-type solutions, whereas the rest take advantage of the limitations of the missile system.

A. Capture Time

The capture time is defined as the time at which the missile reaches a given distance r_f to the aircraft. The performance measure to be maximized is hence the total flight time

$$J(\mathbf{u}) = \int_{t_0}^{t_f} \mathrm{d}t = t_f - t_0 \tag{44}$$

where the free final time is defined by the terminal condition

$$h(\mathbf{x}_f) = r(t_f) - r_f = 0 \tag{45}$$

in which

$$r = \sqrt{(x_a - x_m)^2 + (y_a - y_m)^2 + (h_a - h_m)^2} \tag{46}$$

is the magnitude of the line-of-sight vector from the missile to the aircraft.

B. Closing Velocity

The closing velocity of the missile is the negative of the time derivative of Eq. (46), that is,

$$v_c = -\dot{r} = \mathbf{r} \cdot \mathbf{v}_c / r \tag{47}$$

where the closing velocity vector is given by Eq. (33). The aircraft minimizes the closing velocity at the final distance r_f. The performance measure is thus

$$J(\mathbf{u}) = v_c(t_f) \tag{48}$$

and the terminal constraint $h(\mathbf{x}_f)$ is given by Eq. (45).

C. Miss Distance

The miss distance is the distance between the vehicles at the time of the closest approach, that is, when the closing velocity is zero. The performance measure to be maximized is the final distance between the aircraft and the missile

$$J(\mathbf{u}) = r(t_f) \tag{49}$$

where the final time is defined by

$$h(\mathbf{x}_f) = v_c(t_f) = 0 \tag{50}$$

D. Control Effort

The instantaneous energy consumption of the missile control system is proportional to the magnitude of the lateral acceleration of the missile. Therefore, to be able to exhaust the power supply of the missile control system, the aircraft should maximize the total control effort of the missile

$$J(\mathbf{u}) = \int_{t_0}^{t_f} a(t)\, \mathrm{d}t \tag{51}$$

where

$$a(t) = \sqrt{a_p^2(t) + a_y^2(t)} \tag{52}$$

denotes the total lateral acceleration of the missile. The terminal constraint is again given by Eq. (45).

E. Gimbal Angle

The gimbal angle, that is, the angle between the line-of-sight vector and the missile centerline, is calculated as

$$\lambda = \arccos(\mathbf{e}_r \cdot \mathbf{e}_{\mathrm{cl}}) \tag{53}$$

where $\mathbf{e}_r$ and $\mathbf{e}_{\mathrm{cl}}$ are unit vectors in the directions of the line-of-sight vector from the missile to the aircraft and the centerline axis of the missile, respectively. The latter one is given by

$$\mathbf{e}_{\mathrm{cl}} = \mathbf{e}_{v_m} \cos\alpha_t + \mathbf{e}_a \sin\alpha_t \tag{54}$$

Above, the total angle of attack α_t is calculated by using

$$C_{L_m}(\alpha_t, M(h_m, v_m)) S_m q(h_m, v_m) = m_m(t) a \tag{55}$$

where $C_{L_m}(\cdot)$ is the lift coefficient and S_m is the reference wing area. Because the dependence of the lift force on the total angle of attack is approximately linear over a large portion of the lift curve, the angle of attack is calculated here by using linear extrapolation. The unit vector in the direction of the total lateral acceleration vector equals

$$\mathbf{e}_a = (\mathbf{a}_p + \mathbf{a}_y)/a \tag{56}$$

where $\mathbf{a}_p$ and $\mathbf{a}_y$ denote the pitch and yaw components of the acceleration vector.

The performance measure to be maximized is of the form

$$J(\mathbf{u}) = \lambda(t_f) \tag{57}$$

and the terminal constraint $h(\mathbf{x}_f)$ is given by Eq. (45).

For numerical reasons, we choose to maximize the final gimbal angle instead of its maximum norm. Obviously, it cannot be guaranteed that the gimbal angle always attains its maximum at the missile's target set, whereupon several optimal control problems with various fixed final times should be solved to obtain a globally optimal solution. This, however, would be impractical.

F. Angular Tracking Rate

The angular tracking rate of the missile defined as the rotation of the line-of-sight vector due to the relative velocity is given by

$$\omega = \frac{|\mathbf{r} \times (-\mathbf{v}_c)|}{\mathbf{r} \cdot \mathbf{r}} = \frac{v_c}{r} \sqrt{1 - (\mathbf{e}_r \cdot \mathbf{e}_{v_c})^2} \tag{58}$$

The performance measure to be maximized is of the form

$$J(\mathbf{u}) = \omega(t_f) \tag{59}$$

and the terminal constraint $h(\mathbf{x}_f)$ is given by Eq. (45). Again, we assume that the tracking rate attains its maximum at the missile's target set.

IV. Receding Horizon Control Scheme

In this section, we introduce a receding horizon control scheme for obtaining a near-optimal solution of the problem (40–43) in a feedback form. In the scheme, the control decisions of the aircraft are made at discrete instants $t_k = k\Delta t$, where k is the stage counter and Δt is a time interval between two successive decision instants. At state $\mathbf{x}(t_k)$ and time t_k, the optimal open-loop controls of the aircraft $\mathbf{u}^*(\mathbf{x}(t_k), t)$ over the interval $t \in [t_k, t_k + T]$ that minimize/maximize performance measure

$$\tilde{J}_k(\mathbf{u}) = \int_{t_k}^{t_k+T} L(\mathbf{x}, \mathbf{u}, t)\, \mathrm{d}t + V(\mathbf{x}(t_k + T), t_k + T) \tag{60}$$

subject to

$$\dot{\mathbf{x}} = \mathbf{f}(\mathbf{x}, \mathbf{u}, t), \qquad \mathbf{x}(t_k) = \mathbf{x}_k \tag{61}$$

$$\mathbf{g}(\mathbf{x}, \mathbf{u}, \dot{\mathbf{u}}, \ddot{\mathbf{u}}) \le \mathbf{0} \tag{62}$$

are solved. Then, the state of the system is updated by implementing the resulting optimal controls at the current state and time $\mathbf{u}^*(\mathbf{x}(t_k), t_k)$ for the interval Δt. By repeating the computation at

each decision instant, the controls at each instant are obtained in a feedback form.

In Eq. (60), the integral term corresponds to the accumulated value of the performance measure J over the planning horizon $T > \Delta t$, and V is a cost-to-go function approximating the optimal cost to go from state $\mathbf{x}(t_k + T)$ at time instant $t_k + T$ to the final state $\mathbf{x}_f$. At each decision instant, an estimate for the distance between the vehicles at the end of the planning horizon is computed by using the optimal open-loop controls obtained in the previous instant. If the missile is expected to reach its target set at the end of the planning horizon, V is replaced with the terminal cost function φ, the terminal constraint

$$h(\mathbf{x}(t_k + T)) = 0 \tag{63}$$

is included, and T is set free. In addition, if the estimated time to go exceeds a missile specific threshold, the computation is stopped.

A. Cost-to-Go Approximation

In receding horizon control, the selection of a suitable cost-to-go function is a key issue. Ideally, the cost-to-go function would equal the optimal cost to go commonly referred to as the value function. For simple optimal control problems, it is obtained as the solution of the related Hamilton–Jacobi–Bellman (HJB) partial differential equation [9]. Unfortunately, the HJB equation is practically impossible to solve for the problem at hand. Therefore, an approximation must be used.

Standard approaches for the selection of the approximate cost to go include the problem approximation, the rollout approach, and the heuristic cost-to-go approximation [20]. In the problem approximation, the cost-to-go approximation is based on a solution of a related but simpler problem that is analytically or computationally tractable. In the rollout approach, the cost to go is obtained as the cost of some suboptimal control sequence referred to as base policy. In the heuristic cost-to-go approximation, the cost to go is approximated with a function of the current state and a set of parameters, whose shape can be adjusted by the parameters.

For the problem at hand, efficient base policies are hard to find without extensive simulations. We therefore apply cost-to-go functions derived by the problem approximation and the heuristic cost-to-go approximation that can be evaluated fast with little computational effort. In some cases, we set the cost to go equal to the terminal cost function φ.

1. Capture Time

The integral term of Eq. (60) is now constant T and does not affect the optimal solution. The true cost to go is the remaining flight time, that is, time to go, which is estimated here by dividing the distance to the target set by the closing velocity. Thus, the performance measure is of the form

$$\tilde{J}_k(\mathbf{u}) = (r(t_k + T) - r_f)/v_c(t_k + T) \tag{64}$$

2. Closing Velocity

Obviously, the minimization of the mere closing velocity at the end of the planning horizon results in evasion. We therefore define the cost-to-go function equal to Eq. (48). The eligibility of this choice is also supported by the numerical results in Sec. V.B. The performance measure is of the form

$$\tilde{J}_k(\mathbf{u}) = v_c(t_k + T) \tag{65}$$

3. Miss Distance

Two main elements affecting the performance of the missile are the kinetic energy and the dynamic delay of the guidance channel of the missile [24]. After the propulsive phase, the energy advantage of the missile is, however, rapidly diminished by the aerodynamic drag. It is therefore reasonable for the aircraft to first decrease the energy advantage of the missile by an outrun maneuver. If the outrunning is not sufficient, the aircraft has to take advantage of the dynamic delay of the guidance channel.

Because the maximization of the mere relative distance at the end of the planning horizon results in an outrun maneuver, we again define the cost to go equal to the terminal cost function, obtaining the performance measure

$$\tilde{J}_k(\mathbf{u}) = r(t_k + T) \tag{66}$$

Application of the above performance measure results in solutions where the aircraft tries to outrun the missile at long ranges. At shorter ranges, the presence of the terminal constraint (50) results in a weave maneuver that maximizes the miss distance. The validity of Eq. (66) is again supported by the numerical results presented in Sec. V.B.

4. Control Effort

The integral term of Eq. (60) corresponds now to the value of Eq. (51) over the planning horizon. The cost-to-go function is approximated by integrating the instantaneous lateral acceleration at the end of the planning horizon over the estimated time to go, that is,

$$\tilde{J}_k(\mathbf{u}) = \int_{t_k}^{t_k+T} a(t)\,\mathrm{d}t + a(t_k+T)(r(t_k+T) - r_f)/v_c(t_k+T) \tag{67}$$

5. Gimbal Angle

Here, the cost-to-go function is constructed by noting that the angular tracking rate, contributing to the gimbal angle, is primarily a function of target acceleration. Because the acceleration of the aircraft is typically maximized by diving [1], the trajectories decreasing the altitude of the aircraft are preferred. Hence, in addition to using the terminal cost function, we use a terminal penalty that compels the aircraft to dive. The performance measure is of the form

$$\tilde{J}_k(\mathbf{u}) = \lambda(t_k + T) + (e^{k\gamma_a(t_k+T)} + 1)^{-1} \tag{68}$$

where $k > 0$ defines the steepness of the dive and γ_a denotes the flight path angle of the aircraft. Small values of k result in vertical nose-down breaks whereas larger ones produce more horizontal trajectories. Consequently, small values of k are applicable only with relatively high initial altitudes that permit vertical dive maneuvers.

6. Angular Tracking Rate

We again define the cost to go equal to the terminal cost, which appears to work well especially with longer planning horizons, see Sec. V.B. The performance measure is of the form

$$\tilde{J}_k(\mathbf{u}) = \omega(t_k + T) \tag{69}$$

B. Numerical Solution

The optimal control problems (60–63) can be solved by any direct method [25], where the principal idea is to convert the optimal control problem into a parameter optimization problem that can be solved by a nonlinear programming (NLP) solver [19]. Here, we use the direct shooting method [19], where the conversion is carried out by discretizing the time

$$t_k = t_k^0 < t_k^1 < \cdots < t_k^N = t_k + T \tag{70}$$

and parametering the controls of the aircraft $\mathbf{u}(t_k^i) = \mathbf{u}_i$, where $i = 0, \ldots, N$. The state equations are then integrated explicitly by using the parameterized controls except for the lateral accelerations of the missile where the exact solution is used. Here, the above conversion method results in a relatively small NLP problem since first, the number of control variables is much smaller than the number of state variables, and second, the defect constraints for the state variables are omitted due to the explicit integration of the state equations.

Instead of applying uniform time steps, we define

$$t_k^{i+1} - t_k^i = \Delta t + qi\Delta t, \qquad i = 0, \ldots, N-1 \tag{71}$$

where $q \geq 0$ determines the growth rate of the time interval toward the end of the planning horizon. This enables utilization of a longer planning horizon with less number of control variables which further reduces the size of the resulting NLP problem.

The resulting NLP problem can be stated as minimize/maximize the objective function

$$F(\mathbf{u}_0, \ldots, \mathbf{u}_{N-1}) = \sum_{i=0}^{N-1} L(\bar{\mathbf{x}}_i, \mathbf{u}_i, t_k^i)(t_k^{i+1} - t_k^i) + V(\bar{\mathbf{x}}_N, t_k^N) \tag{72}$$

subject to

$$\mathbf{g}(\bar{\mathbf{x}}_i, \mathbf{u}_i, \dot{\mathbf{u}}_i, \ddot{\mathbf{u}}_i) \leq \mathbf{0}, \qquad i = 0, \ldots, N \tag{73}$$

$$h(\bar{\mathbf{x}}_N) = 0 \tag{74}$$

where the state of the system at t_k^{i+1}, denoted by $\bar{\mathbf{x}}_{i+1}$, is obtained by integrating the state equations (61) one time step forward with a suitable explicit numerical integration technique by applying the control vector $\mathbf{u}_i$ with the initial state $\bar{\mathbf{x}}_i$, where $\bar{\mathbf{x}}_0 = \mathbf{x}_k$. Constraints (73) and (74) refer to Eqs. (62) and (63), respectively, where the control rate and acceleration vectors denoted by $\dot{\mathbf{u}}_i$ and $\ddot{\mathbf{u}}_i$ are approximated by finite differences as described in the following. Terminal constraint (74) is included only if the missile is expected to reach its target set at the end of the planning horizon. Then, a uniform step length is applied where the length of the interval is specified by the free final time.

The control rate and angular acceleration constraints (11–14) are handled approximatively as follows. The first and the second time derivatives of the angle of attack and the bank angle are replaced by finite difference approximations. By substituting the approximations into Eqs. (11–14), the following constraints for consecutive values of the angle of attack and the bank angle are obtained at time instant t_k^i:

$$\frac{\alpha_{i+1} - \alpha_i}{t_k^{i+1} - t_k^i} + \dot{\bar{\gamma}}_{a,i} \cos\mu_i + \dot{\bar{\chi}}_{a,i} \cos\bar{\gamma}_{a,i} \sin\mu_i - Q_{\max} \leq 0 \tag{75}$$

$$-\frac{\alpha_{i+1} - \alpha_i}{t_k^{i+1} - t_k^i} - \dot{\bar{\gamma}}_{a,i} \cos\mu_i - \dot{\bar{\chi}}_{a,i} \cos\bar{\gamma}_{a,i} \sin\mu_i - Q_{\max} \leq 0 \tag{76}$$

$$\frac{\mu_{i+1} - \mu_i}{t_k^{i+1} - t_k^i} - P_{\max}(\alpha_i, \bar{h}_{a,i}, M(\bar{h}_{a,i}, \bar{v}_{a,i})) \leq 0 \tag{77}$$

$$-\frac{\mu_{i+1} - \mu_i}{t_k^{i+1} - t_k^i} - P_{\max}(\alpha_i, \bar{h}_{a,i}, M(\bar{h}_{a,i}, \bar{v}_{a,i})) \leq 0 \tag{78}$$

and

$$\frac{\alpha_{i+1} - 2\alpha_i + \alpha_{i-1}}{(t_k^{i+1} - t_k^i)^2} - \ddot{\alpha}_{\max} \leq 0 \tag{79}$$

$$-\frac{\alpha_{i+1} - 2\alpha_i + \alpha_{i-1}}{(t_k^{i+1} - t_k^i)^2} - \ddot{\alpha}_{\max} \leq 0 \tag{80}$$

$$\frac{\mu_{i+1} - 2\mu_i + \mu_{i-1}}{(t_k^{i+1} - t_k^i)^2} - \dot{P}_{\max} \leq 0 \tag{81}$$

$$-\frac{\mu_{i+1} - 2\mu_i + \mu_{i-1}}{(t_k^{i+1} - t_k^i)^2} - \dot{P}_{\max} \leq 0 \tag{82}$$

The control rate limits will be satisfied only approximatively, because they are nonlinear with respect to the state variables. The accuracy of the approximation can be improved by using shorter integration time steps.

V. Numerical Examples

In this section, the receding horizon control scheme is demonstrated with the performance measures introduced in Sec. IV. In the first example, solutions related to each performance measure are illustrated with the optimal open-loop trajectories. Convergence of the receding horizon solutions toward the optimal open-loop ones is also demonstrated. In the second example, receding horizon and optimal open-loop solutions for a set of initial states are visualized with level curves. In the third example, the computation times and the quality of the receding horizon solutions are analyzed by comparing them to the optimal open-loop ones.

The aircraft and the missile models correspond to a generic fighter aircraft and a generic medium range air-to-air missile. The initial values of the angle of attack, bank angle, and throttle setting are set to $\alpha_0 = 0$, $\mu_0 = 0$, and $\eta_0 = 1$, respectively. The maximum angle of attack, maximum pitch rate, and maximum angular accelerations of the angle of attack and bank angle are set to $\alpha_{\max} = 32$ deg, $Q_{\max} = 25$ deg s^{-1}, $\ddot{\alpha}_{\max} = 40$ deg s^{-2}, $\dot{P}_{\max} = 120$ deg s^{-2}. The minimum altitude, maximum dynamic pressure, and maximum load factor of the aircraft are initialized to $h_{a,\min} = 500$ m, $q_{\max} =$ 80 kPa, and $n_{a,\max} = 9$, respectively. The navigation constant and maximum load factor of the missile are set to $N' = 4$ and $n_{m,\max} = 40$, respectively. The aircraft employs an afterburner. The thrust force of the missile is defined as

$$T_m(t) = \begin{cases} T_b, & 0 \leq t \leq 3 \text{ s} \\ T_s, & 3 < t \leq 8 \text{ s} \\ 0, & t > 8 \text{ s} \end{cases} \tag{83}$$

Consequently, the mass of the missile $m_m(t)$ first decreases piecewise linearly and remains thereafter constant.

We set $\Delta t = 0.25$ s, $q = 0.25$, and $N = 2, 4, 6$ that according to Eq. (71) results in the planning horizons of $T_2 = 0.56$ s, $T_4 = 1.38$ s, and $T_6 = 2.44$ s, respectively. For a better performance, Δt is doubled in the maximization of the control effort, which also doubles the length of the planning horizon. In Eq. (68), we set $k = 100$. Except for the miss distance maximization, the final distance between the aircraft and the missile is initialized to $r_f = 100$ m.

In the NLP problem (72–74), the state equations are integrated numerically with the explicit Euler's method. At each decision instant, the state of the system is updated by using the fourth-order Runge–Kutta method [25] which is also applied in the solution of the optimal open-loop solutions by the direct multiple shooting method. In the open-loop optimization, equidistant integration steps are used. The step size is determined by the initial iterate computed by the receding horizon control scheme. Because the final time is free, the step size does not necessarily coincide with the interval Δt, but remains nearby it. The NLP problems are solved with SNOPT [26] solver that uses a sequential quadratic programming (SQP) algorithm [27]. The computations are performed by using a desktop computer equipped with a 3.20 GHz clock frequency Pentium D CPU and 2 GB of memory.

A. Example 1

At first, we analyze receding horizon and optimal open-loop solutions for a single initial state. The initial altitudes and the velocities of the aircraft and the missile are $h_{a_0} = h_{m_0} = 6000$ m and $v_{a_0} = v_{m_0} = 250$ ms^{-1}, respectively. We also set $x_{m_0} = 10,000$ m, $x_{a_0} = 0$, $y_{a_0} = y_{m_0} = 0$, and $\gamma_{a_0} = \gamma_{m_0} = 0$. The initial headings of the aircraft and the missile are set to $\chi_{a_0} = 45$ deg and

$\chi_{m_0} = 178$ deg. Hence, the missile is launched toward the aircraft with a small lead angle.

The optimal open-loop trajectories of the aircraft and the missile for the different performance measures are presented in Fig. 1. Figure 1a illustrates that the maximization of the capture time results in a trajectory in which the aircraft immediately turns away from the closing missile and tries to outrun it. Comparison to Figs. 1b and 1c reveals that irrespective of the utilized performance measure, the solutions are similar except for the endgame. In the minimization of the closing velocity as well as in the maximization of the miss distance, the aircraft starts to weave in the end, whereupon the missile must use larger lateral acceleration. This increases the missile drag force which in turn decreases the closing velocity. On the other hand, a weave maneuver initiated at the proper time before the interception maximizes the miss distance due to the dynamic lag in the missile guidance system [7].

With the other three performance measures, the aircraft tends to fly toward the closing missile instead of outrunning as illustrated in Figs. 1d–1f. In the maximization of the control effort, the aircraft curves toward the missile which compels the missile to attain relatively large lateral accelerations over the duration of the flight. In the maximization of the gimbal angle, the aircraft tries to increase its acceleration by diving as well as to maintain the bearing perpendicular to the missile during the flight. The missile must use large lateral accelerations during the last second of the flight which increases the gimbal angle in the end. The maximization of the tracking rate results in a similar solution. In the end, the aircraft performs a high-g roll maneuver that rapidly increases the tracking rate.

To summarize, the aircraft dives in the optimal solutions irrespective of the performance measure as presented in Fig. 1. This is understandable, because the drag of the missile is increased at lower altitudes. Because the limitations of the missile can be best exploited with low closing velocities, the reason for decreasing the altitude is obvious. The aircraft also avails larger thrust force at lower altitudes which is useful considering the outrunning of the missile. The solutions accord with usual evasive tactics performed by the fighter pilots where a typical maneuver consists of an immediate break turn followed by a dive maneuver and weaving during the endgame [1].

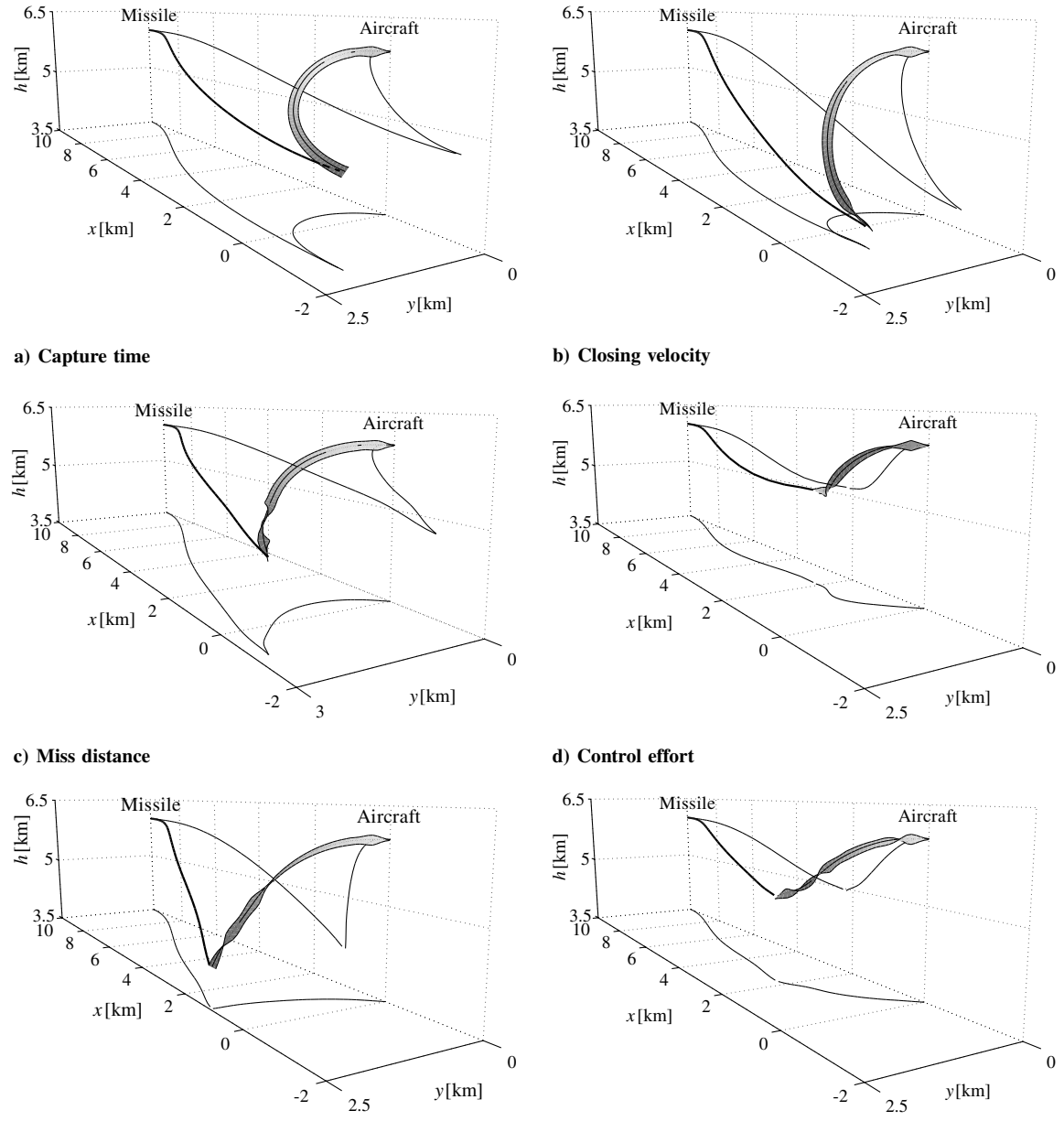

a) Capture time **b) Closing velocity**

c) Miss distance **d) Control effort**

e) Gimbal angle **f) Tracking rate**

Fig. 1 Optimal open-loop trajectories with different performance measures.

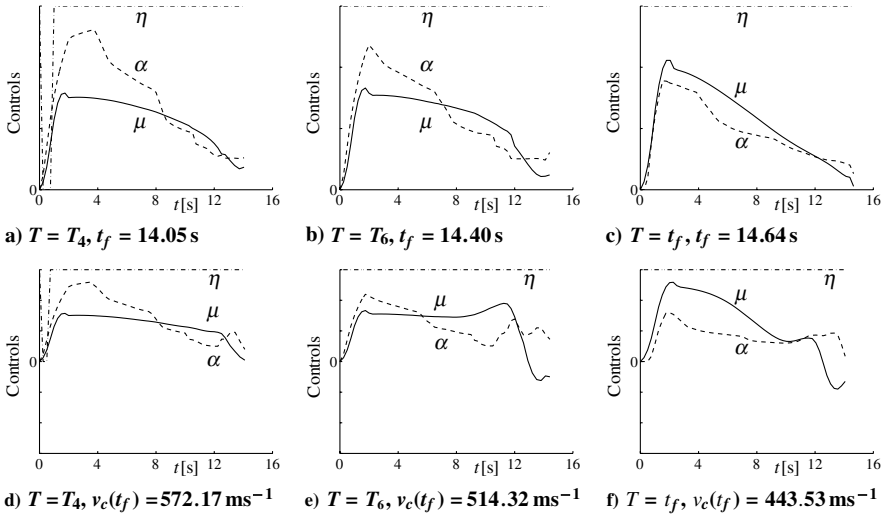

a) $T = T_4$, $t_f = 14.05$ s b) $T = T_6$, $t_f = 14.40$ s c) $T = t_f$, $t_f = 14.64$ s

d) $T = T_4$, $v_c(t_f) = 572.17\ \mathrm{ms}^{-1}$ e) $T = T_6$, $v_c(t_f) = 514.32\ \mathrm{ms}^{-1}$ f) $T = t_f$, $v_c(t_f) = 443.53\ \mathrm{ms}^{-1}$

Fig. 2 Control histories of the aircraft; capture time a)–c), closing velocity d)–f). The maximum levels of α, μ, and η equal 32 deg, 180 deg, and 1.0.

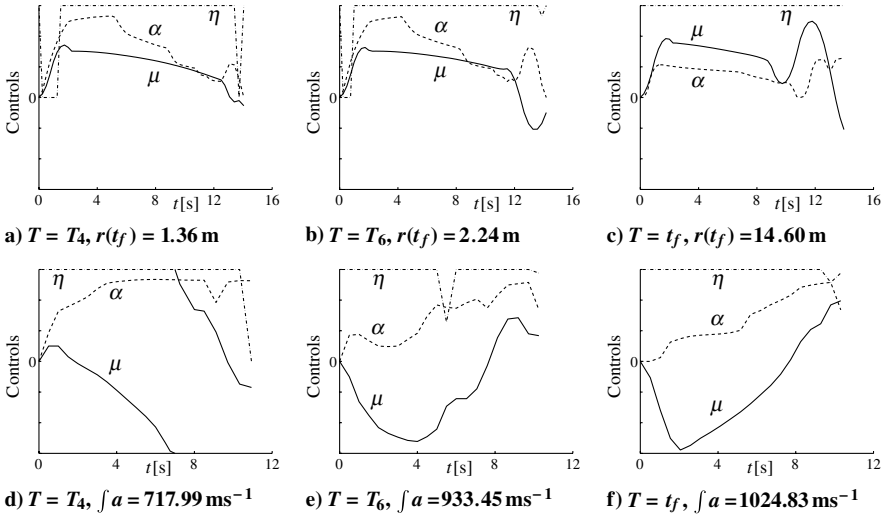

a) $T = T_4$, $r(t_f) = 1.36$ m b) $T = T_6$, $r(t_f) = 2.24$ m c) $T = t_f$, $r(t_f) = 14.60$ m

d) $T = T_4$, $\int a = 717.99\ \mathrm{ms}^{-1}$ e) $T = T_6$, $\int a = 933.45\ \mathrm{ms}^{-1}$ f) $T = t_f$, $\int a = 1024.83\ \mathrm{ms}^{-1}$

Fig. 3 Control histories of the aircraft; miss distance a)–c), control effort d)–f). The maximum levels of α, μ, and η equal 32 deg, 180 deg, and 1.0.

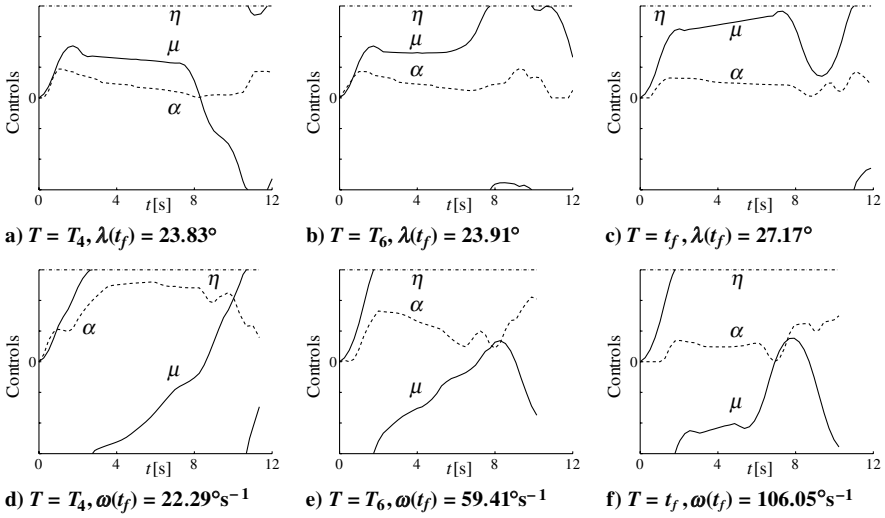

a) $T = T_4$, $\lambda(t_f) = 23.83°$ b) $T = T_6$, $\lambda(t_f) = 23.91°$ c) $T = t_f$, $\lambda(t_f) = 27.17°$

d) $T = T_4$, $\omega(t_f) = 22.29°\mathrm{s}^{-1}$ e) $T = T_6$, $\omega(t_f) = 59.41°\mathrm{s}^{-1}$ f) $T = t_f$, $\omega(t_f) = 106.05°\mathrm{s}^{-1}$

Fig. 4 Control histories of the aircraft; gimbal angle a)–c), tracking rate d)–f). The maximum levels of α, μ, and η equal 32 deg, 180 deg, and 1.0.

The receding horizon controls of the aircraft with the planning horizons T_4 and T_6 as well as the optimal open-loop controls are presented in Figs. 2–4. Figures 2–4 indicate convergence toward the optimal open-loop solution as the planning horizon is extended. In most cases, efficient solutions are obtained already with a short planning horizon. However, short planning horizons do not appear to work well in the maximization of the miss distance and the tracking rate; see the values of the performance measures in Figs. 3a, 3b, 4a,

and 4b. This is intuitively clear especially in the first case, where the proper initiation and the duration of the endgame evasion maneuver is critical. A short planning horizon along with the utilized cost-to-go approximation simply do not allow long enough endgame evasion maneuvers to achieve acceptable miss distances. It should be noted that in the optimal solution for the miss distance maximization, the load factor limit (17) prevents the saturation of the angle of attack to its upper bound in the endgame.

B. Example 2

Let us next analyze solutions computed for a set of initial states described in the following. The initial states are the same as in Example 1 except for the distance and the headings. The missile is launched toward the aircraft at the distances of $x_{m_0} = 2000, 3000, \ldots, 20{,}000$ m, where the initial headings of the aircraft are set to $\chi_{a_0} = 0, 15, \ldots, 180$ deg for each range. Consequently, the number of initial states equals 247. The initial headings of the missile are given by

$$\chi_{m_0} = 180 \text{ deg} - \arcsin\frac{v_a \sin\chi_{a_0}}{v_m} e^{-0.0003(x_{m_0}-2000)} \tag{84}$$

where the arcsine term corresponds to the theoretical lead angle which would lead the missile to the nominal collision point if the aircraft and the missile continued to fly along straight-line paths at constant velocities [7]. Here, we use $v_a = v_{a_0}$ and $v_m = 2v_{m_0}$ to anticipate the increase in the velocity of the missile due to the boost and sustain phases. The exponential term in Eq. (84) decreases the lead angle as the launch distance is increased.

In Figs. 5–7, level curves of the receding horizon and optimal open-loop solutions are presented. In the figures, the aircraft lies in the origin and flies to the right. The missile is launched toward the aircraft with an appropriate lead angle. The initial range and direction of the missile are given by r and θ, respectively. Since suboptimality of the solutions would result in somewhat serrated level curves, the computed performance levels are approximated by suitable continuous and smooth functions. Because of the approximation, the boundaries of the envelopes are not necessarily precisely accurate.

Figures 5a–5c indicate that in the maximization of the capture time, solutions of good quality are obtained with a short planning horizon irrespective of the launch range and launch direction. According to Fig. 5c, the maximum launch range of the missile is 11–16 km depending on the launch direction. The launch range is largest for a head-on launch and smallest when the missile is launched directly behind the aircraft.

Figures 5d and 5f suggest similar results for the minimization of the closing velocity as above. Near-optimal solutions are again achieved with a short planning horizon. Note that the optimal closing velocity peaks at the launch range of about 5 km. At shorter ranges, the duration of the encounter falls below the boost and sustain time of the missile. Consequently, the missile does not achieve its maximal velocity which decreases the closing velocity. Comparison of Figs. 5c and 5f indicates that the maximization of the capture time and the minimization of the closing velocity yield almost similar maximum launch ranges.

In the maximization of the miss distance, the miss distances fall notably below the optimal ones with a short planning horizon (see Figs. 6a and 6c). This is evident especially for the front sector launches. However, with short ranges where the speed advantage of the missile is not yet overwhelming, miss distances near the optimal ones are obtained also with a short planning horizon. As the planning horizon is extended, the achieved miss distances close on the optimal open-loop ones (see Figs. 6b and 6c). Figures 6a–6c indicate that the miss distances are smallest if the missile is launched almost head-on at the range of 5–10 km.

A short planning horizon does not appear to yield efficient solutions in the maximization of the control effort (see Fig. 6d). However, extending the planning horizon again improves the performance level as illustrated in Fig. 6e. Comparison to Fig. 6f reveals that the gap to the open-loop optimal solutions is still notable. Figure 6f indicates that in general, larger control efforts are achieved for rear sector launches when the aircraft flies initially away from the missile.

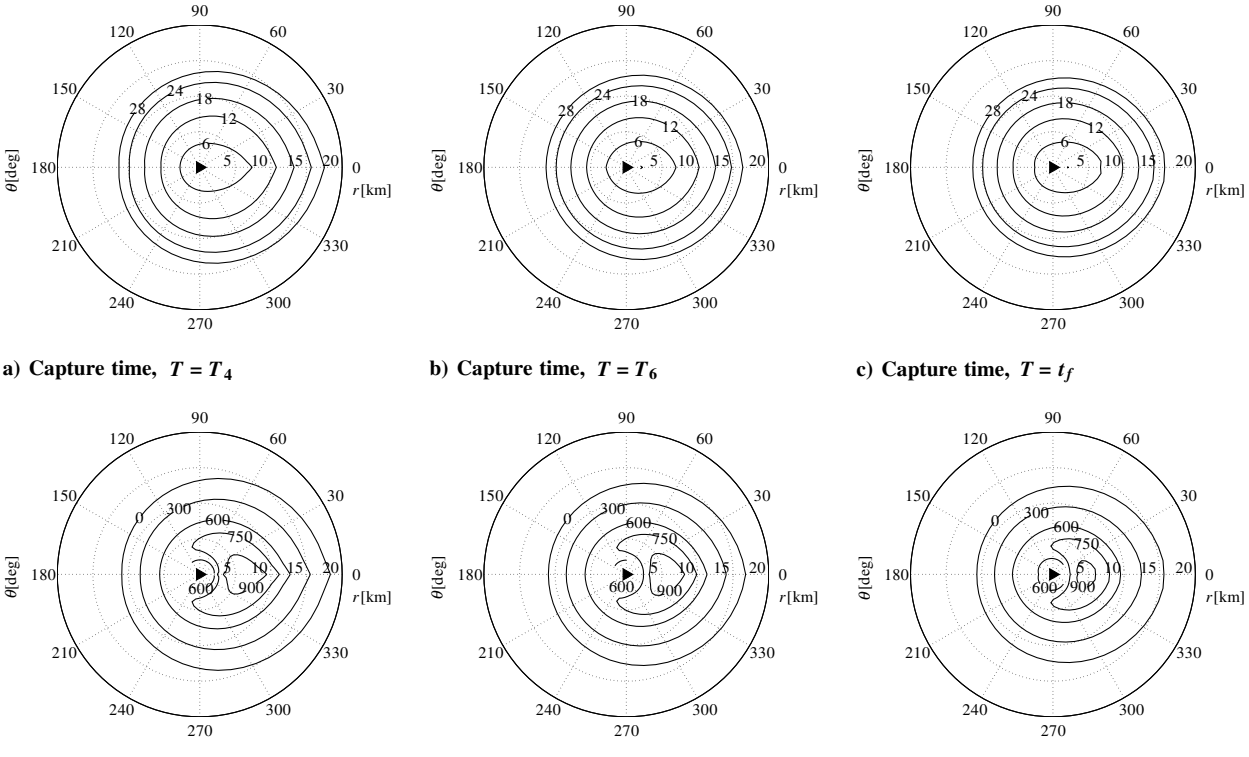

a) Capture time, $T = T_4$ b) Capture time, $T = T_6$ c) Capture time, $T = t_f$

d) Closing velocity, $T = T_4$ e) Closing velocity, $T = T_6$ f) Closing velocity, $T = t_f$

Fig. 5 Level curves of the optimal capture time and closing velocity. The numbers above the horizontal axis refer to the initial range r, whereas θ denotes the direction of launch.

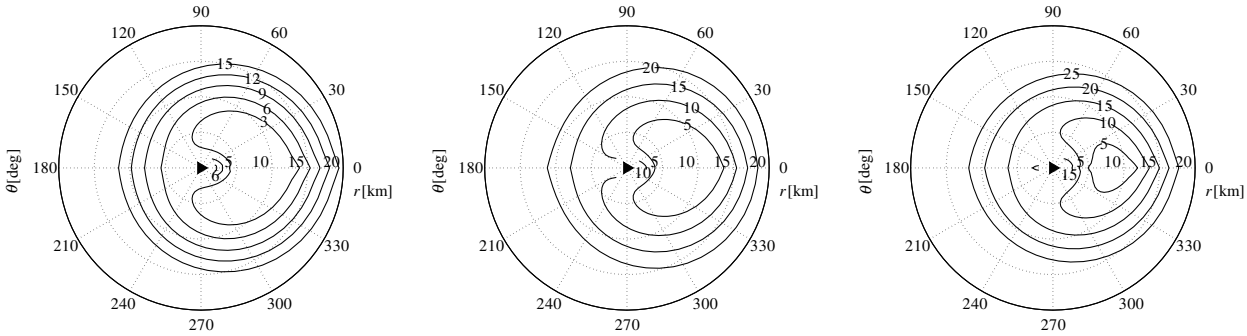

a) Miss distance, $T = T_4$ b) Miss distance, $T = T_6$ c) Miss distance, $T = t_f$

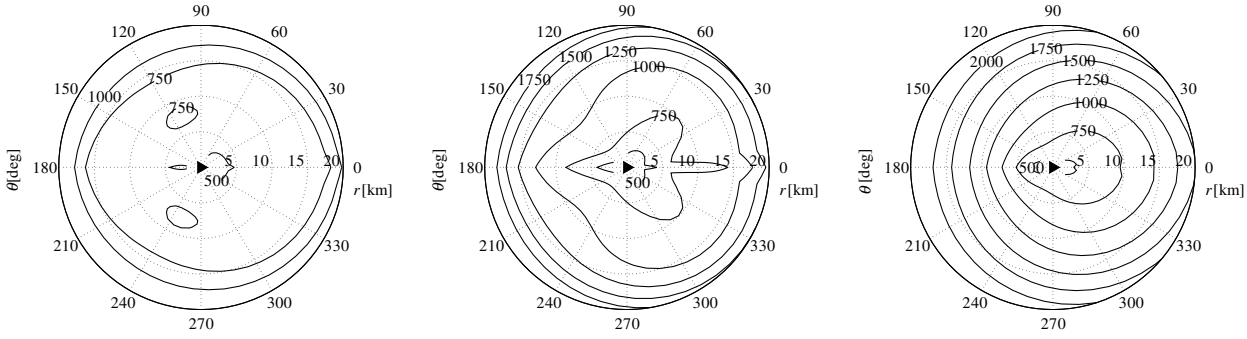

d) Control effort, $T = T_4$ e) Control effort, $T = T_6$ f) Control effort, $T = t_f$

Fig. 6 Level curves of the optimal miss distance and control effort. The numbers above the horizontal axis refer to the initial range r, whereas θ denotes the direction of launch.

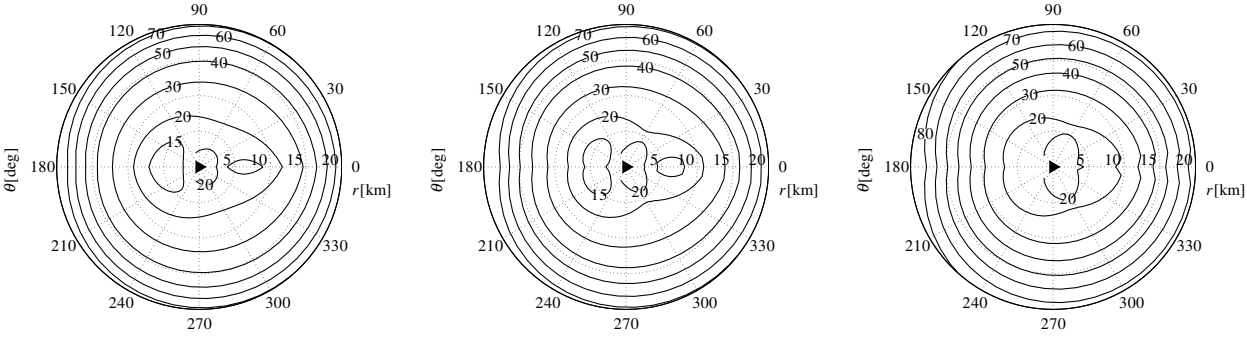

a) Gimbal angle, $T = T_4$ b) Gimbal angle, $T = T_6$ c) Gimbal angle, $T = t_f$

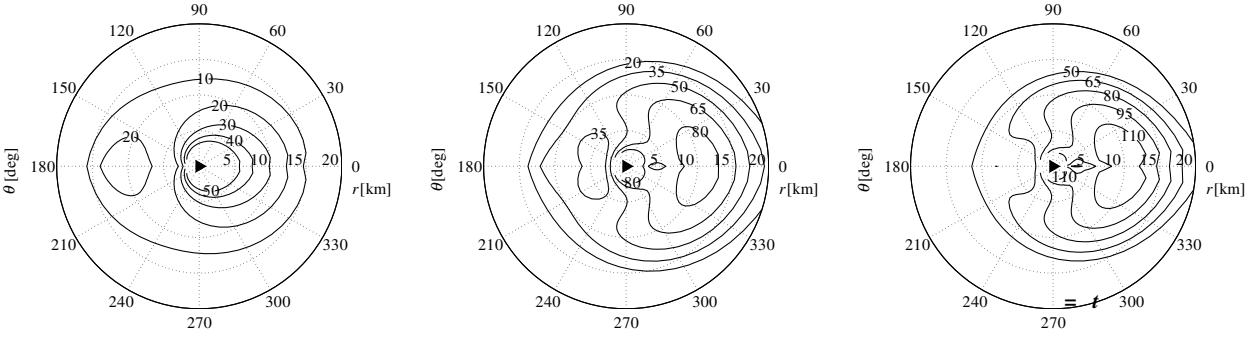

d) Tracking rate, $T = T_4$ e) Tracking rate, $T = T_6$ f) Tracking rate, $T = t_f$

Fig. 7 Level curves of the optimal gimbal angle and tracking rate. The numbers above the x axis refer to the initial range r, whereas θ denotes the direction of launch.

Figures 7a–7c suggest that in the maximization of the gimbal angle, near-optimal solutions are again achieved with a short planning horizon. Figures 7a–7c indicate that the maximum gimbal angle depends mainly on the launch range.

Considering the maximization of the tracking rate, Fig. 7d indicates that a short planning horizon provides efficient solutions for short launch ranges, but not for longer ones. However, application of a longer planning horizon improves the quality of the solutions also

Table 1 Average computation times per decision instant and average performance losses

Criterion	T_2		T_4		T_6	
	$\bar{t}$, s	$\bar{\epsilon}$	$\bar{t}$, s	$\bar{\epsilon}$	$\bar{t}$, s	$\bar{\epsilon}$
Capture time	0.044	0.030	0.096	0.022	0.219	0.009
Closing velocity	0.044	0.117	0.098	0.105	0.222	0.094
Miss distance	0.027	0.591	0.084	0.425	0.232	0.219
Control effort	0.045	0.319	0.159	0.314	0.447	0.161
Gimbal angle	0.035	0.143	0.147	0.142	0.389	0.097
Tracking rate	0.036	0.701	0.127	0.565	0.316	0.267

for longer launch ranges (see Fig. 7e). Figures 7e and 7f indicate that the limit can be best exceeded if the missile is launched from the front sector, that is, when the closing velocity is high whereas nearby rear sector launches are more devastating.

To summarize, near-optimal solutions are obtained even with a short planning horizon for such performance measures as the capture time, closing velocity, and gimbal angle. For the rest of the analyzed performance measures, a longer planning horizon is required. In light of the numerical results, the missile can be avoided most successfully when it is launched from the rear sector. The obvious reason is that the aircraft is then flying away from the missile. In general, the obtained solutions appear to be realistic and converge to the optimal open-loop ones.

C. Example 3

We next analyze the performance of the scheme with the different planning horizons. For a performance measure J and a given initial state, the performance loss of a receding horizon solution is defined as

$$\epsilon = \frac{|J(\mathbf{u}^\circ) - J(\mathbf{u}^*)|}{\max\{J(\mathbf{u}^*), J(\mathbf{u}^\circ)\}} \tag{85}$$

where $\mathbf{u}^\circ$ denotes the receding horizon solution and $\mathbf{u}^*$ is the optimal open-loop solution. Instead of using $J(\mathbf{u}^\circ)$ in the denominator of Eq. (85), we apply $\max\{J(\mathbf{u}^*), J(\mathbf{u}^\circ)\}$, which makes the definition symmetric with respect to minimization and maximization problems, see [28]. Consequently, the performance loss ϵ obtains values between 0 and 1 for both kinds of problems. The average performance loss is obtained by taking the average of Eq. (85) over the initial states defined in Example 2 for which the missile reaches its target set. The average computation times per decision instant along with the average performance losses are presented in Table 1 for the planning horizons T_2, T_4, and T_6.

The results presented in Table 1 support the conclusions drawn in Example 2. For the capture time, closing velocity, and gimbal angle, the average performance losses are small even with a short planning horizon which means that the obtained receding horizon solutions are near optimal on the average. With the other performance measures, a longer planning horizon is required. Note that the average performance losses decrease as the planning horizon is extended, so the solutions apparently converge to the optimal open-loop ones. In addition, the average computation times per decision instant remain feasible considering real-time implementation of the scheme.

VI. Implementation Aspects

In practice, the introduced computation scheme could be used as part of a guidance system of an unmanned aerial vehicle, in the guidance model of a batch air combat simulator, or in a pilot advisory system. In these settings, the scheme would provide near-optimal feedback controls with respect to a given performance measure. Concerning the selection of the most suitable performance measure for a given combat state, the performance measure could be selected by ranking the solutions according to the optimal values of the respective performance measures and choosing the best one. For example, if the missile is launched outside its kinematic range, the capture time and the closing velocity would be ranked first and either of them would hence be selected. The optimal values of the different performance measures for the current combat state could be obtained by using off-line computed launch state maps similar to those presented in Example 2. It should be noted that in general, the optimal value of the performance measure depends on the size of the missile's target set, which should be taken into account in the generation of the launch state maps. This applies especially for the gimbal angle and the tracking rate, where better values are achieved with shorter final distances, and vice versa.

From the practical point of view, the assumption about the accurate state information is optimistic. In reality, a radar warning receiver usually gives a relatively good idea of the direction of the missile that has been launched but fails to provide accurate range information. Probably the best estimate on the range of the missile is often obtained by a radar acquisition of the launching platform at the moment of firing, see [1].

The detection of the platform provides information for maneuvering according to a worst case scenario in which it is assumed that a highly capable missile is launched toward the aircraft at the time of acquisition, see [14]. In this scenario, the controls of the aircraft are optimized against the presumed threat. This is continued until more reliable information about the state of the missile is acquired at a certain range, after which the updated missile's state is fed into the receding horizon control scheme. In practice, the state of the missile could be estimated from the uncertain measurements by using, for example, the extended Kalman filter.

On the other hand, the range and relative velocity information received by the missile is prone to errors as well. Especially, low altitude and look-down of the missile expose the radar of the missile's seeker system to ground clutter which may cause it to totally lose a track of the target aircraft [29]. Although these aspects are not considered in this paper, they could be taken into account in the scheme by suitable cost-to-go approximations inducing dive maneuvers.

It is evident that in practical settings, avoidance tactics depend strongly on the type and the guidance law of the missile. Because of the uncertainty regarding these issues, the assumptions about them should be updated as the missile closes on the aircraft. For example, the assumption about the guidance law could be represented as a discrete probability distribution over a set of predefined guidance laws. The probability distribution could then be updated on the basis of different features derived from the trajectories of the vehicles using a similar Bayesian network than in [5,6]. Suitable features include the angle between the line-of-sight vector and the velocity vector of the missile, and distance of the missile from the guideline directed from the launcher to the target aircraft. Because the values of the above features are typically distinct for different guidance laws, they provide the basis for the updating. The Bayesian network could also be extended to cover the uncertainty regarding the missile type as well. Obviously, the measurement of the above features can be challenging. The estimates for the features could be obtained from the state measurements by using the extended Kalman filter which could also be incorporated in the Bayesian network [30].

It should be noted that due to the computational delay, the controls related to a particular initial time of a truncated horizon optimization problem are outdated when the optimization is finished. Therefore, instead of applying the first controls of the optimal control sequence, one should implement the controls related to a particular initial time plus the computational delay. Moreover, one could continue using the obtained control sequence until the new one is available.

The computational delay could be possibly decreased by constructing effective base policies, that is, predefined suboptimal control sequences, and using them as initial iterates in the solution of the NLP problem (72–74). For example, in the miss distance maximization the optimal endgame maneuver is typically a weave maneuver initiated at the proper instant. These policies could be computed off-line for different time to go's and closing velocities and use them as initial iterates in the scheme. This could effectively shorten the convergence times of the SQP algorithm, enabling the utilization of longer planning horizons with reasonable computation times.

It is possible that the applied cost-to-go approximations produce locally optimal solutions. For example, in Fig. 1d, the aircraft flies toward the missile although in general, larger control efforts are obtained for rear sector launches (see Fig. 6f). This implies the possibility of another local optimum where the aircraft at first turns away from the missile. Also, in short range head-on settings, near-optimal solutions could possibly be obtained by flying toward the missile and performing a suitable endgame maneuver. Cost-to-go approximations resulting in these kinds of solutions could be constructed for different settings on the basis of the optimal open-loop solutions. For example, turning away from the missile can be induced, for example, by maximizing the relative distance between the vehicles.

In this paper, the vehicle dynamics are modeled by using point-mass models but also more complex aerodynamic models could be applied as well. This would obviously increase the computational burden because a short integration step is required for realistic modeling of the rotation dynamics. It should also be pointed out that the accuracy of the optimal open-loop solutions over the planning horizon is not crucial, because only the first controls or the initial part of the obtained control sequence are applied at each decision instant.

In the aircraft model applied in this paper, the angle of attack and the roll acceleration limits are assumed constant. In principle, rotational dynamics could be approximated by the first-order transfer functions with suitable time constants. Consequently, at a particular state, for example, the maximum roll acceleration would be given as a function of the current and maximum roll rates. However, this would result in an intractable optimization model due to the massively increased nonlinearity of the control constraints. Moreover, the computation scheme and the vehicle models presented in the paper appear to produce sufficiently realistic solutions concerning the utilization of the guidance scheme in practice.

Finally, the missile model could be expanded by introducing a more realistic autopilot model. For example, if the exceeding of the gimbal angle limit is imminent, the lock-off could be tried to be prevented by adding an intentional bias signal to the guidance command. In addition, it is possible to append various loft schemes in the autopilot model.

VII. Conclusions

A new computation scheme based on receding horizon control is introduced and applied in the solution of a pursuit–evasion problem between a medium range air-to-air missile and a fighter aircraft. As a result, near-optimal controls of the aircraft are obtained in feedback form. In the computation scheme, the optimal open-loop controls of the aircraft over a truncated planning horizon are solved at each decision instant by the direct shooting method. For short planning horizons, the computation can be carried out in real time by a desktop computer. The numerical results presented in the paper indicate that application of even relatively short planning horizons results in efficient solutions with such performance measures as the capture time, closing velocity, and gimbal angle. For the miss distance, tracking rate, and control effort of the missile, a planning horizon of several seconds is required. The introduced scheme could be used, for example, as a part of a guidance system of an unmanned aerial vehicle as well as in the guidance model of a batch air combat simulator, or in a pilot advisory system. In addition to air-to-air missile avoidance, the scheme could also be applied in surface-to-air missile encounters.

References

[1] Shaw, R. L., *Fighter Combat: Tactics and Maneuvering*, Naval Institute Press, Annapolis, MD, 1985, pp. 46–48, 58–60.

[2] Breitner, M. H., "Robust Optimal Onboard Reentry Guidance of a Space Shuttle: Dynamic Game Approach and Guidance Synthesis via Neural Networks," *Journal of Optimization Theory and Applications*, Vol. 107, No. 3, 2000, pp. 481–503.

[3] García, C. E., Prett, D. M., and Morari, M., "Model Predictive Control: Theory and Practice—Survey," *Automatica*, Vol. 25, No. 3, 1989, pp. 335–348.

[4] Richalet, J., Rault, A., Testud, L., and Papon, J., "Model Predictive Heuristic Control: Applications to Industrial Processes," *Automatica*, Vol. 14, No. 5, 1978, pp. 431–428.

[5] Virtanen, K., Raivio, T., and Hämäläinen, R. P., "Modeling Pilot's Sequential Maneuvering Decisions by a Multistage Influence Diagram," *Journal of Guidance, Control, and Dynamics*, Vol. 27, No. 4, 2004, pp. 665–677.

[6] Virtanen, K., Karelahti, J., and Raivio, T., "Modeling Air Combat by a Moving Horizon Influence Diagram Game," *Journal of Guidance, Control, and Dynamics*, Vol. 29, No. 5, 2006, pp. 1080–1091.

[7] Zarchan, P., *Tactical and Strategic Missile Guidance*, Vol. 176, Progress in Astronautics and Aeronautics, 3rd ed., AIAA, Reston, VA, 1997, pp. 12, 15, 104.

[8] Raivio, T., "Capture Set Computation of an Optimally Guided Missile," *Journal of Guidance, Control, and Dynamics*, Vol. 24, No. 6, 2001, pp. 1167–1175.

[9] Bryson, A. E., and Ho, Y., *Applied Optimal Control*, Hemisphere Publishing Corp., New York, 1975, pp. 42–89, 148–176.

[10] Ong, S. Y., and Pierson, B. L., "Optimal Planar Evasive Aircraft Maneuvers Against Proportional Navigation Missiles," *Journal of Guidance, Control, and Dynamics*, Vol. 19, No. 6, 1996, pp. 1210–1215.

[11] Shinar, J., Rotsztein, Y., and Bezner, E., "Analysis of Three-Dimensional Optimal Evasion with Linearized Kinematics," *Journal of Guidance and Control*, Vol. 2, No. 5, 1979, pp. 353–360.

[12] Imado, F., and Uehara, S., "High-g Barrel Roll Maneuvers Against Proportional Navigation from Optimal Control Viewpoint," *Journal of Guidance, Control, and Dynamics*, Vol. 21, No. 6, 1998, pp. 876–881.

[13] Imado, F., "Some Aspects of a Realistic Three-Dimensional Pursuit-Evasion Game," *Journal of Guidance, Control, and Dynamics*, Vol. 16, No. 2, 1993, pp. 289–293.

[14] Karelahti, J., Virtanen, K., and Raivio, T., "Game Optimal Support Time of a Medium Range Air-to-Air Missile," *Journal of Guidance, Control, and Dynamics*, Vol. 29, No. 5, 2006, pp. 1061–1069.

[15] Imado, F., and Miwa, S., "Fighter Evasive Maneuvers Against Proportional Navigation Missile," *Journal of Aircraft*, Vol. 23, No. 11, 1986, pp. 825–830.

[16] Singh, L., "Autonomous Missile Avoidance Using Nonlinear Model Predictive Control," *Proceedings of the AIAA Guidance, Navigations, and Control Conference*, AIAA, Reston, VA, Aug. 2004, pp. 1–15; also AIAA Paper 2004-4910.

[17] Shneydor, N. A., *Missile Guidance and Pursuit: Kinematics, Dynamics and Control*, Horwood Publishing, Chichester, England, 1998, pp. 171–196.

[18] Raivio, T., and Ranta, J., "Miss Distance Maximization in the Endgame," *Proceedings of the AIAA Guidance, Navigation, and Control Conference*, AIAA, Reston, VA, Aug. 2002, pp. 1–11; also AIAA Paper 2002-4947.

[19] Hull, D. G., "Conversion of Optimal Control Problems into Parameter Optimization Problems," *Journal of Guidance, Control, and Dynamics*, Vol. 20, No. 1, 1997, pp. 57–60.

[20] Bertsekas, D. P., *Dynamic Programming and Optimal Control*, Vol. 1, 2nd ed., Athena Scientific, Belmont, MA, 2000, pp. 297–344.

[21] Betts, J. T., "Survey of Numerical Methods for Trajectory Optimization," *Journal of Guidance, Control, and Dynamics*, Vol. 21, No. 2, 1998, pp. 193–207.

[22] Miele, A., *Flight Mechanics: Theory of Flight Paths*, Vol. 1, Addison–Wesley, Reading, MA, 1962, pp. 48–50.

[23] Yuan, P.-J., and Chern, J.-S., "Ideal Proportional Navigation," *Journal of Guidance, Control, and Dynamics*, Vol. 15, No. 5, 1992, pp. 1161–1165.

[24] Shinar, J., and Tabak, R., "New Results in Optimal Missile Avoidance Analysis," *Journal of Guidance, Control, and Dynamics*, Vol. 17, No. 5, 1994, pp. 897–902.

[25] Betts, J. T., *Practical Methods for Optimal Control Using Nonlinear Programming*, Advances in Design and Control, Society for Industrial and Applied Mathematics, Philadelphia, PA, 2001, pp. 63–91.

[26] Gill, P. E., Murray, W., and Saunders, M. A., "SNOPT: An SQP Algorithm for Large-Scale Constrained Optimization," *SIAM Review*, Vol. 47, No. 1, 2005, pp. 99–131.

[27] Bertsekas, D. P., *Nonlinear Programming*, Athena Scientific, Belmont, MA, 1995, pp. 372–382.

[28] Papadimitriou, C. M., *Computational Complexity*, Addison Wesley, Reading, MA, 1994, p. 300.

[29] Miwa, S., Imado, F., and Kuroda, T., "Clutter Effect on the Miss Distance of a Radar Homing Missile," *Journal of Guidance, Control, and Dynamics*, Vol. 11, No. 4, 1988, pp. 336–342.

[30] Jensen, F. V., *Bayesian Networks and Decision Graphs, Statistics for Engineering and Information Science*, Springer, New York, 2001, p. 65.